


FULL PAPER

Open Access



Asymmetric deformation of the Earth's magnetosphere under low Alfvén Mach number solar wind: Observations and MHD simulation

Masaki N. Nishino^{1,2,3*} , Hiroshi Hasegawa², Yoshifumi Saito², Benoit Lavraud⁴, Yukinaga Miyashita^{5,6}, Motoharu Nowada⁷, Satoshi Kasahara¹ and Tsugunobu Nagai⁸

Abstract

The density of the solar wind plasma near the Earth's magnetosphere sometimes decreases to only several per cent of the usual value, and such density extrema result in a significant reduction of the dynamic pressure and Alfvén Mach number (M_A) of the solar wind flow. While a symmetric expansion of the Earth's magnetosphere by the low dynamic pressure was assumed in previous studies, a global magnetohydrodynamic (MHD) simulation study predicted a remarkable dawn-dusk asymmetry of the magnetospheric shape under low-density solar wind and Parker-spiral interplanetary magnetic field (IMF) configuration. Here, we present observations consistent with the asymmetric deformation of the magnetosphere under low- M_A solar wind and Parker-spiral IMF conditions, focusing on the significant expansion of the dawn-flank magnetosphere detected by the Geotail spacecraft. A global MHD simulation reproduced the dawnward expansion of the near-Earth magnetosphere, which was consistent with the observation by Geotail. The solar wind flow had a non-negligible dusk-to-dawn component and partly affected the dawnward expansion of the magnetosphere. Local, roughly Alfvénic sunward acceleration of magnetosheath ions at the dawn flank magnetopause suggests magnetosheath plasma entry into the magnetosphere through open field lines generated by magnetic reconnection at the dayside magnetopause. At the same time, Cluster 1 and 3, located near the southern polar cusp, also detected continuous antisunward ion jets and occasional sunward jets, which are consistent with the occurrence of magnetic reconnection near the southern cusp. These observations suggest that enhanced plasma acceleration at the dayside magnetopause operates under the low- M_A solar wind and Parker spiral IMF conditions and that plasma influx across the dawnside magnetopause is at work under such a low- M_A condition. These results can be helpful in understanding interactions between low- M_A solar/stellar winds and celestial objects, such as inner planets and exoplanets.

Keywords: Low density solar wind, Earth's magnetosphere, Alfvén Mach number, Solar wind–magnetosphere interaction

*Correspondence: nishino@stp.isas.jaxa.jp

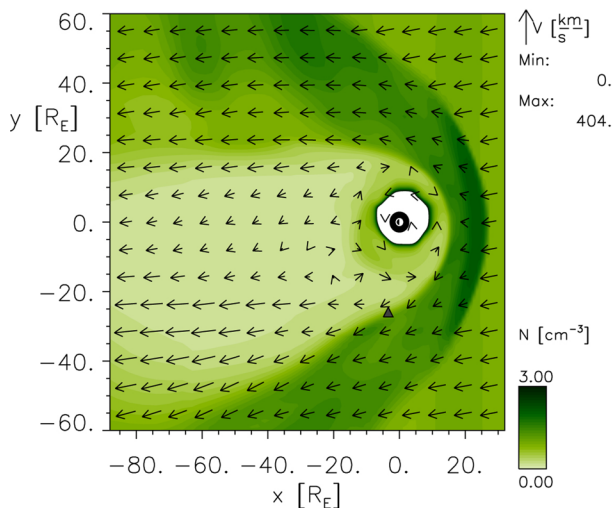
¹ Department of Earth and Planetary Science, Graduate School of Science, University of Tokyo, 7-3-1 Hongo, Bunkyo-ku, Tokyo 113-0033, Japan
Full list of author information is available at the end of the article

Graphic Abstract

Dawn-dusk asymmetric magnetosphere reproduced by a global MHD simulation

02/11/2007 Time = 14:30:00 UT $z = 0.00R_E$

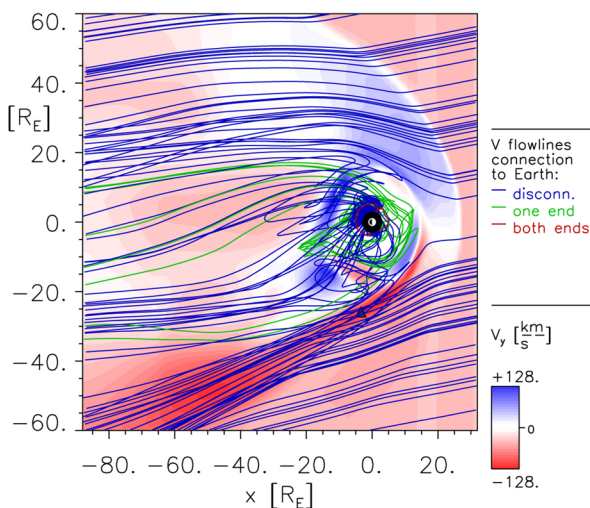
▲Geotail



Model at CCMC: BATSRUS

02/11/2007 Time = 14:30:00 UT $z = 0.00R_E$

▲Geotail



Model at CCMC: BATSRUS

Introduction

The solar wind flow near the Earth’s orbit is almost always super-Alfvénic so that a fast-mode bow shock forms in front of the Earth’s magnetosphere. The normal solar wind conditions around the Earth’s magnetosphere (i.e. plasma density of several cm^{-3} , solar wind speed of $\sim 400\text{--}500$ km/s, and strength of the interplanetary magnetic field (IMF) of several nT) give a typical Alfvén Mach number (M_A) of 5–10, where M_A is defined as the ratio of solar wind speed to Alfvén speed. However, previous studies reported that the Alfvén Mach number at times becomes lower than 2 and even as low as ~ 1 (Le et al. 2000; Fairfield et al. 2001; Watari et al. 2001; Lavraud et al. 2007; Lavraud and Borovsky 2008; Nishino et al. 2008; Chané et al. 2012). The low- M_A solar wind condition has been known to potentially cause a significant effect on the magnetospheric response (Lavraud et al. 2007; Lavraud and Borovsky 2008; Kataoka and Miyoshi 2008), while the small number of events has prevented us from entirely understanding the phenomena. The terrestrial magnetospheric profiles under low- M_A conditions can be helpful for the discussion of plasma processes at the inner planets in the solar system (Slavin and Holzer 1981) and moons of giant planets (Jia and Kiverson 2021). In addition to the solar system objects, the interaction between low- M_A stellar winds and exoplanets may also result in a similar response of the exoplanetary

magnetosphere. Some exoplanets have been found in regions close to the central star, where the stellar wind might not be fully accelerated to the supersonic flow and thus the stellar wind passing by the exoplanetary magnetosphere might have a low M_A (Lugaz et al. 2016). Finally, the interstellar medium also shows an interaction with an obliquely directed magnetic field with a lower M_A , giving rise to an asymmetry around it (Miniati et al. 1999).

In our previous paper (Nishino et al. 2008) on the interaction between the low- M_A solar wind ($M_A \sim 2$) and the Earth’s magnetosphere, we reported a strong flow deflection toward dusk at the dayside bow shock under Parker spiral (B_X and B_Y dominant) IMF based on the Geotail observations. The global magnetohydrodynamic (MHD) simulation shown in Nishino et al. (2008) was in agreement with the in-situ observations in the dayside magnetosheath with respect to the plasma flow deflection. This MHD simulation study predicted an expansion of the magnetotail toward dawn under a low M_A of ~ 2 . In summary, simulation studies showed that the obliquely directed magnetic field yields a dawn-dusk asymmetry around an obstacle under low- M_A condition (Chapman et al. 2004; Nishino et al. 2008). However, no previous study was dedicated to in situ observations of the dawn-side magnetopause under the low- M_A and Parker spiral IMF conditions.

In this paper, we report a prolonged low- M_A solar wind event with the Parker-spiral IMF on February 11, 2007, when Geotail was located near the magnetopause boundary layer on the dawnside and Cluster crossed the high-latitude magnetopause in the southern hemisphere. We analyse magnetopause boundary crossing data from Geotail and indicate plasma entry from the magnetosheath to the lobe/mantle region along open field lines. Based on Geotail observations and a global MHD simulation, we show significant deformation of the magnetosphere expanding toward dawn under low- M_A solar wind and obliquely directed IMF conditions. We also present Cluster observations of associated continuous magnetic reconnection at the dayside magnetopause.

Instrumentation

We use 12-s averaged ion data obtained by the LEP (Low Energy Particle) experiment onboard Geotail (Mukai et al. 1994). Ion measurement by the LEP-EAi instrument covers an energy-per-charge range of 32 eV/q to 39 keV/q. Electron energy-time spectrograms from 8 eV to 38 keV from LEP-EAe are also shown for reference. We mainly use the particle count data compressed into two-dimensional data around the spacecraft spin axis that is nearly parallel to the Z direction of the Geocentric Solar Ecliptic (GSE) coordinate system. We also use the three-dimensional ion phase space density that is available only for limited periods. Magnetic field data are obtained at a sampling rate of 16 Hz (Kokubun et al. 1994), and 12-s averaged data are used in this study.

We also use Cluster data; ion data from CIS (Cluster Ion Spectrometry)-HIA (Hot Ion Analyzer; Dandouras (2010); Rème et al. (1997)), electron energy-time spectrograms from PEACE (Plasma Electron And Current Experiment; Fazakerley (2010); Johnstone et al. (1997)), and spin-averaged magnetic field data from the fluxgate magnetometer (FGM) instrument (Balogh et al. 1997). The ion energy-per-charge range of the CIS observations is from ~ 5 eV/e to 32 keV/e, and the electron energy range of PEACE is from 0.59 eV to 26.4 keV.

The solar wind data from the Wind spacecraft are provided by NASA. We also use the solar wind electron and ion data from the 3DP instrument (Lin et al. 1995) and magnetic field data from the MFI instrument (Lepping et al. 1995) onboard the Wind spacecraft (Acuña et al. 1995).

The Geocentric Solar Magnetospheric (GSM) coordinate system is mainly used for describing the spacecraft data and the MHD simulation results, while the GSE coordinate system is partly used.

Solar wind observations by Wind

On February 11, 2007, the solar wind speed observed by the Wind spacecraft was as slow as 280 km/s, and its density was ~ 1.0 cm $^{-3}$ until 17:30 UT. The combination of the solar wind speed and density gave a very low dynamic pressure of ~ 0.14 nPa (Fig. 1f), which is only several per cent of the typical value (~ 2.1 nPa). The averaged IMF between 12:00 and 17:00 UT was (4.5, -4.6 , -0.2) nT in GSM with a strength of 6.5 nT. These parameters yielded an Alfvén Mach number (M_A) as low as ~ 2.0 (Fig. 1e) and a very low β value (the ratio of ion thermal to magnetic pressure) of 0.14.

We note that the solar wind flow had a non-negligible dusk-to-dawn component; The bulk plasma flow averaged over 12:00 and 17:00 UT was (-274 , -53 , -21) km/s in GSM. The large dusk-to-dawn component of the bulk solar wind flow under the low-density condition is consistent with a previous study on the 11 May 1999 event by Janardhan et al. (2005), who suggested that the low-density solar wind flow was a corotating stream and thus had a significant downward component. The solar wind flow had a slight negative (southward) component, which may cause the entire magnetotail to move southward.

Geotail observations at dawn flank

Figure 2 shows an overview of Geotail observations for 12 hours from 10:00 to 22:00 UT. Until 11:37 UT Geotail was in the southern hemisphere of the magnetosphere and observed the plasma sheet with an ion temperature of ~ 1 keV. The locations of the Geotail spacecraft at 11:37 UT and at 18:30 UT in the GSE coordinate system were (-5.0 , -26.1 , -1.7) R_E and (-1.3 , -28.2 , -2.9) R_E , respectively (Fig. 3). After 11:37 UT Geotail stayed in the magnetopause boundary layer between the magnetospheric plasma sheet, the lobe/mantle, and the magnetosheath, and detected anti-sunward (tailward) ion flows of 100 to 400 km/s repeatedly until 18:30 UT. The outbound magnetopause crossing around 18:30 UT was caused by a compression of the magnetosphere due to the recovery of the solar wind density. A number of jumps in the anti-sunward flow velocity correlated with changes in the magnetic field orientation correspond to magnetopause crossings. They are consistent with ion influx from the magnetosheath into the magnetotail through open field lines, which will be discussed later.

In Fig. 3, we simply rotated the model magnetopause for a solar-wind dynamic pressure of 0.14 nPa around the GSE- Z axis, taking into account the aberration of the magnetotail by the non-negligible solar wind

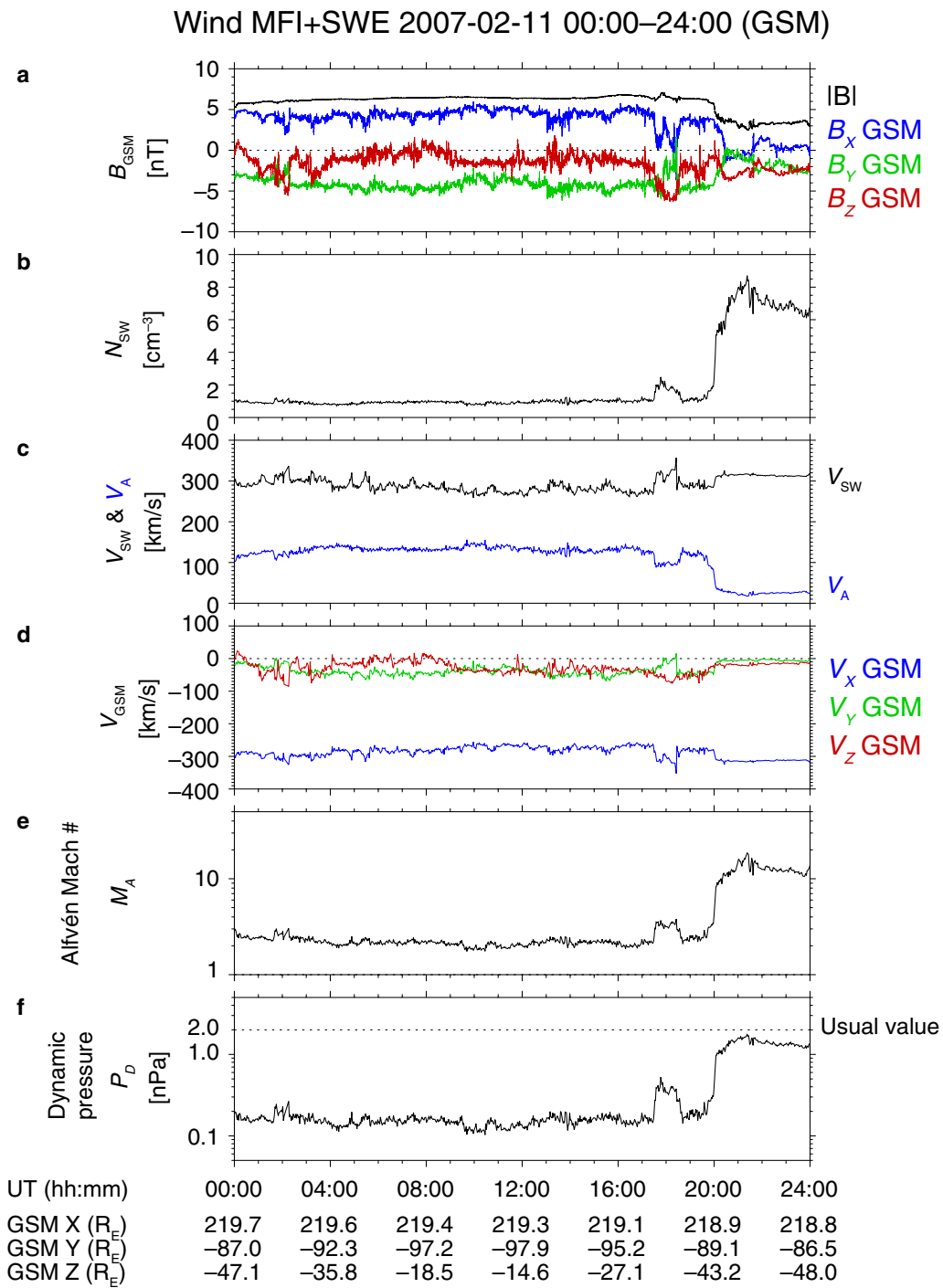
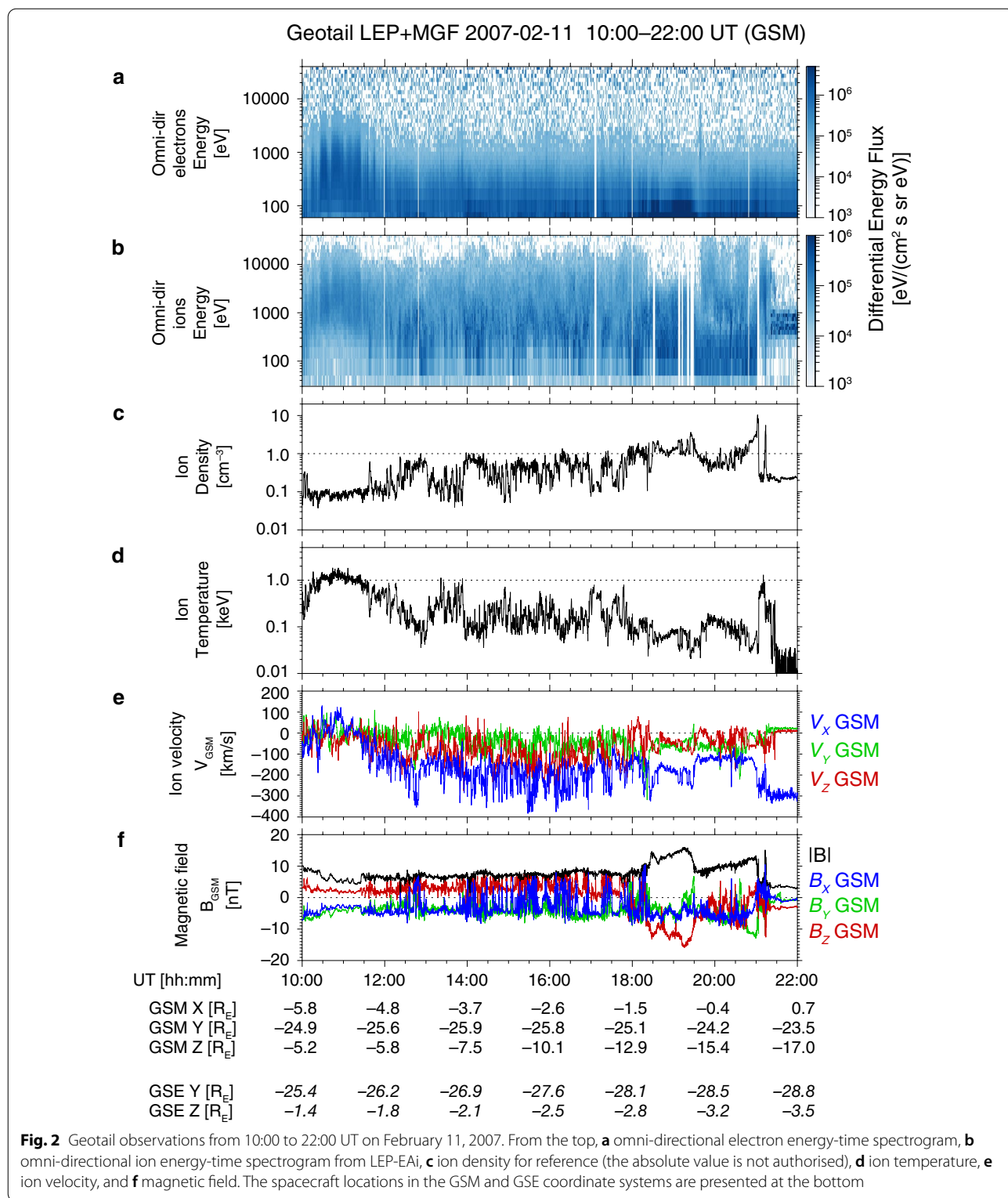


Fig. 1 Solar wind data obtained by the Wind spacecraft on February 11, 2007. From the top, **a** magnetic field, **b** ion density, **c** solar wind bulk speed (black) and Alfvén speed (blue), **d** ion velocity, **e** Alfvén Mach number, and **f** dynamic pressure are plotted. The GSM coordinate system is used for the magnetic field, velocity, and spacecraft locations



V_Y component (-53 km/s) and the Earth’s revolution (29.8 km/s). We have found that the magnetopause detected by Geotail was more than $5 R_E$ outward of the

model magnetopause location even though an effect of the solar-wind aberration toward dawn is considered.

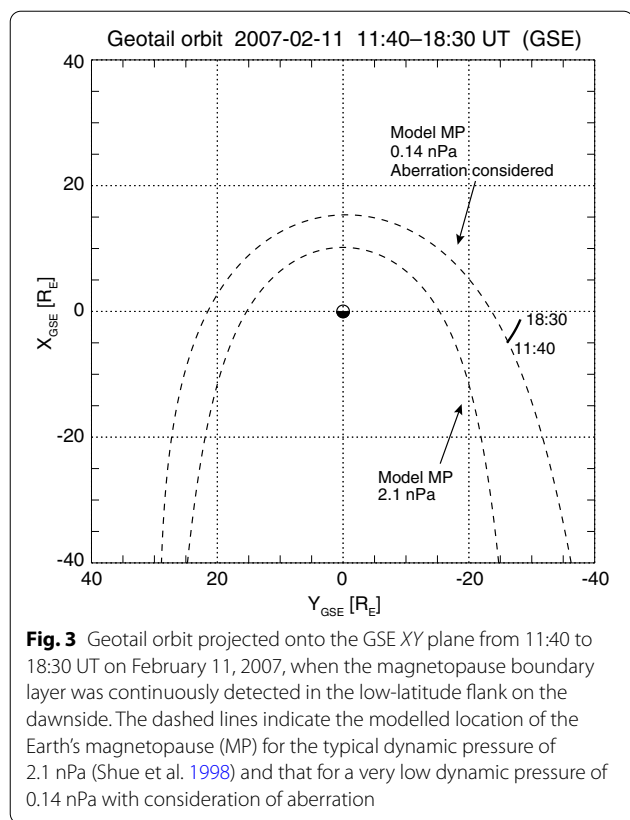


Figure 4 shows expanded data for 3.5 hours from 13:30 to 17:00 UT when Geotail was mostly in the magnetopause boundary layer. In the boundary layer, the plasma flowed in the anti-sunward (tailward) direction with a speed of $\sim 100\text{--}200$ km/s (i.e. lobe/mantle-like region), and faster anti-sunward flows of 300–400 km/s (i.e. magnetosheath-like region) were detected occasionally (Fig. 4d and g). During multiple boundary crossings between 14:30 and 15:10 UT, the density and temperature were anti-correlated, and denser plasma roughly coincided with faster anti-sunward flows and magnetic field variations. The magnetic field intensity did not show significant change during encounters with the faster anti-sunward ion flows, while B_Z dominated the other two components. Power spectral densities of V_X (Fig. 4h) enhanced in the frequency range of 1 to several mHz (i.e. Pc5 range), which corresponds to semi-periodical encounters of fast anti-sunward ion flows in the magnetopause boundary layer.

Similar encounters with faster anti-sunward ion flows repeatedly occurred until the outbound magnetopause crossing at 18:30 UT. The lobe/mantle-like regions with a smaller anti-sunward velocity and a higher ion temperature were detected occasionally. The formation of the lobe/mantle region in the southern hemisphere at the

dawnside tail-flank under the dawnward and southward IMF conditions (i.e. $B_Y < 0$ and $B_Z < 0$) is consistent with previous statistical study in the distant magnetotail (See Figs. 7 and 10 in Hasegawa et al. (2002a)). The typical ion temperature in such a region (e.g. around 17:10 UT) was ~ 500 eV, which means that the cold plasma sheet and the thick low-latitude boundary layer were not formed in this event. No detection of high-energy electrons during this event suggests that Geotail stayed on open field lines or once-opened field lines.

We examined the high-speed anti-sunward ion flows to obtain further information on their origin and properties. Since the three-dimensional phase space density of ions are available after 16:28:25 UT on the day, we expand 16-min data between 16:30–16:46 UT including typical high-speed anti-sunward flows (Fig. 5). In this period, an anti-sunward ion flow was enhanced in the 24 s period between 16:37:51–16:38:15 UT (corresponding to the 2 data sets of the LEP-EAi instrument). The ion phase space density for the 24 s period (Figs 6a–c) shows that the fast anti-sunward ions are most likely to be the magnetosheath flow. The ion flow velocity was $(-304, -72, -138)$ km/s in GSM, and its speed was ~ 340 km/s. The ion phase space density obtained in the slower region between 16:36:03–16:36:15 UT (Figs. 6d–f) shows typical lobe/mantle characteristics.

We performed the Walén analysis (Sonnerup et al. 1987) to investigate the nature of the fast anti-sunward flows at the magnetopause boundary. Figure 7 shows the results of the Walén analysis for the 5-min period between 16:36:03–16:41:03 UT, which includes both the faster magnetosheath-like flow and the slower lobe/mantle-like flow mentioned above. For this period, the de Hoffmann-Teller frame velocity (V_{HT}) is estimated to be $(-242, -136, -49)$ km/s in GSM, and the correlation coefficient (*c.c.*) between the plasma velocity in the de Hoffman-Teller frame ($V - V_{HT}$) and the local Alfvén velocity (V_A) is as large as -0.97 . The moderately large Walén slope (~ -0.5) is consistent with the view that the magnetopause has all properties of a rotational discontinuity and the magnetosheath plasma thus locally enters the lobe/mantle region through open field lines. The magnitude of the slope significantly lower than unity could be explained by several effects as discussed by Hasegawa et al. (2002b). The negative correlation indicates that the normal component of the magnetic field at the rotational discontinuity of the magnetopause was directed outward (anti-earthward).

The flow vector in the lobe/mantle region at 16:36:03 UT was $(-176, -37, -99)$ km/s in GSM and $(66, 99, -50)$ km/s in the de Hoffmann-Teller frame. The sunward flow direction of the lobe/mantle ions in

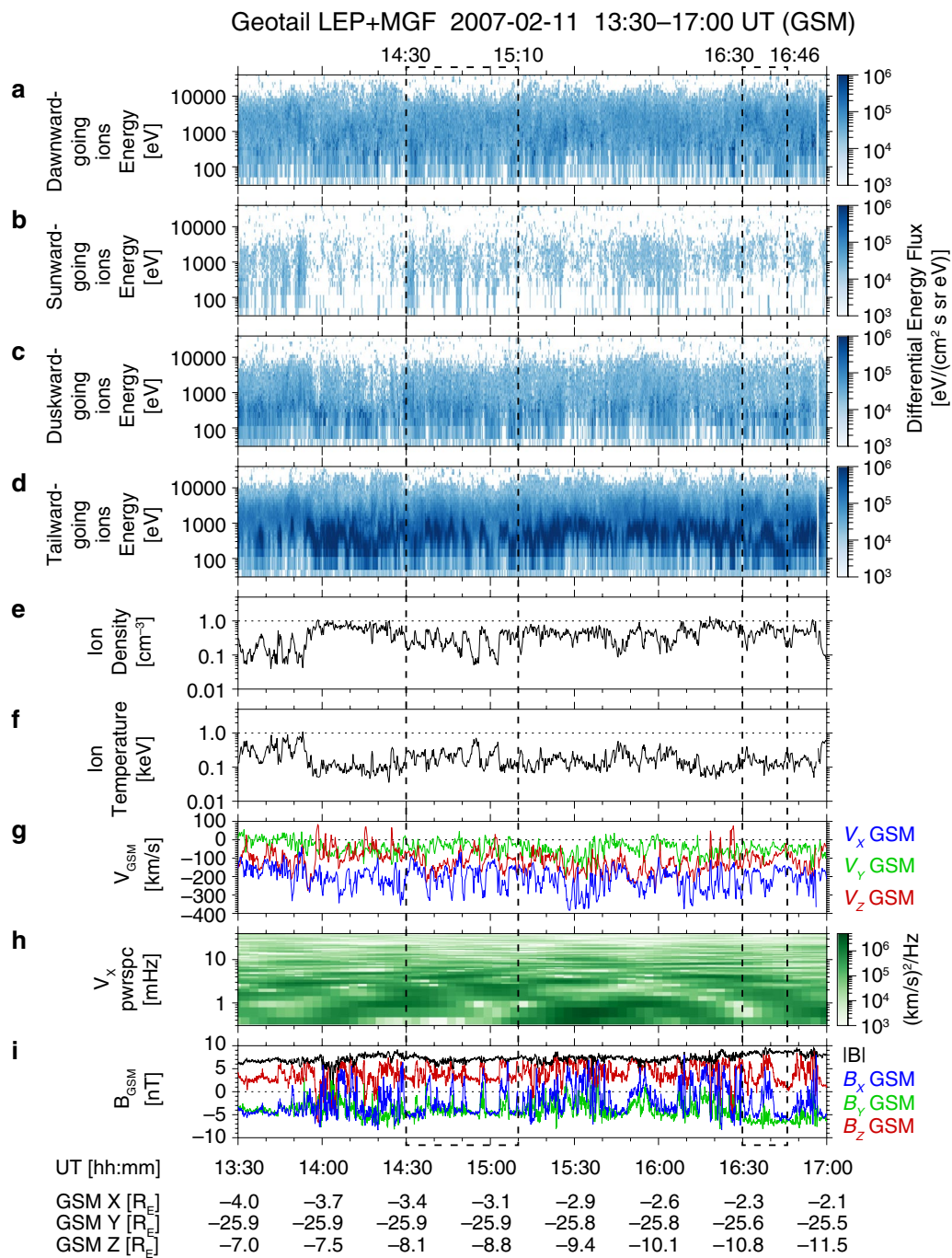


Fig. 4 An expansion of the Geotail observation for 3.5 hours from 13:30 to 17:00 UT. Energy-time spectrograms for **a** dawnward-going ions, **b** sunward-going ions, **c** duskward-going ions, **d** antisunward-going ions, **e** ion density, **f** ion temperature, **g** ion velocity in GSE, **h** power spectral density of V_x , and **i** magnetic field in GSE are plotted. The former rectangle between 14:30–15:10 UT corresponds to the period with detailed explanations of the boundary properties (See main text), while the latter between 16:30–16:46 UT corresponds to the period expanded in Fig. 5

the de Hoffmann-Teller frame suggests a deceleration through the entry from the magnetosheath into the magnetotail by the sunward Lorentz force ($\mathbf{J} \times \mathbf{B}$) acting on a bulk plasma, which is consistent with the outward

normal component of the magnetic field at the rotational discontinuity.

We applied the same procedure to other 17 faster anti-sunward flow encounters between 13:30–17:00 UT

Geotail LEP+MGF 2007-02-11 16:30–16:46 UT (GSM)

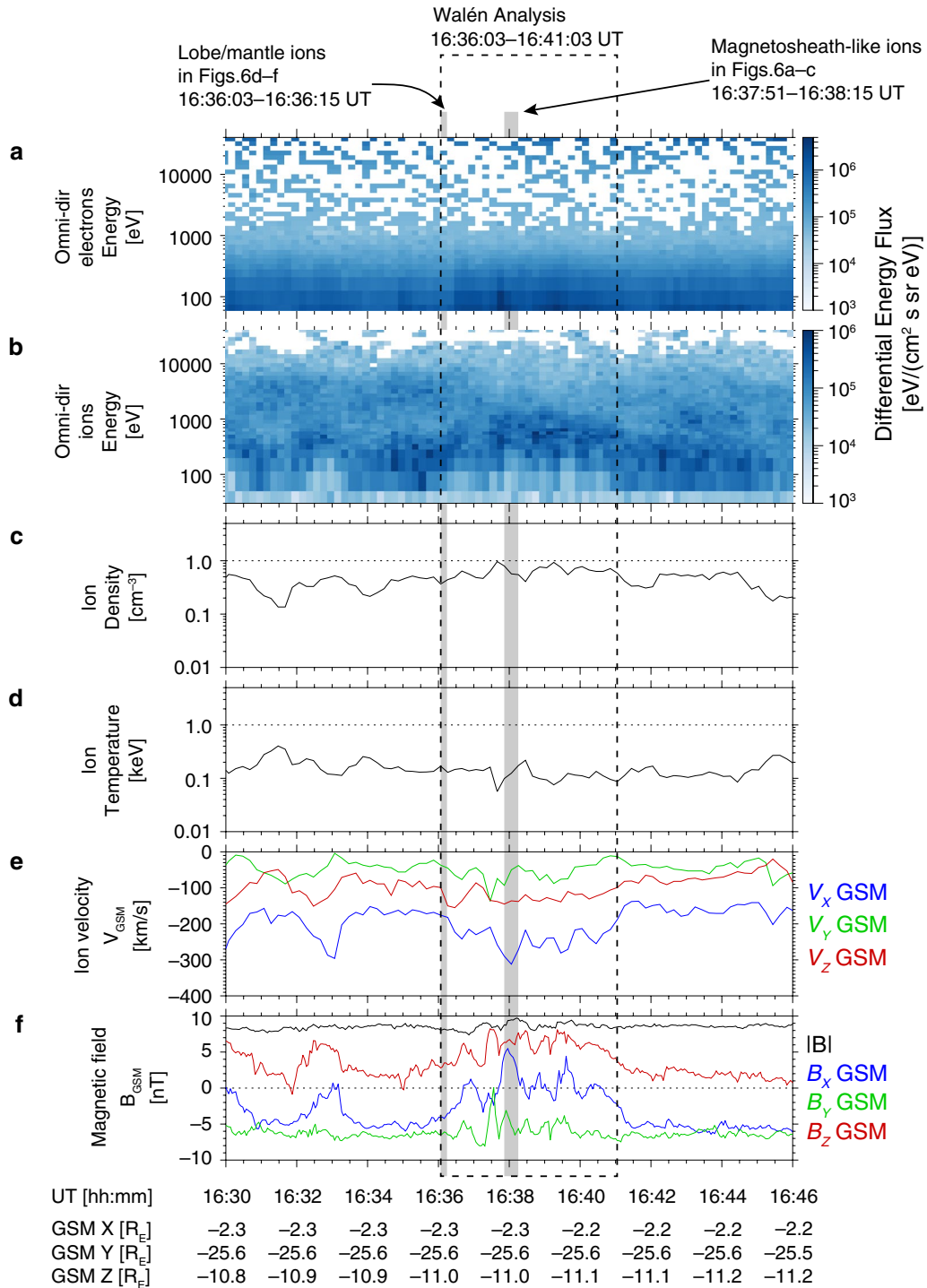


Fig. 5 An expansion of the Geotail observations from 16:30 to 16:46 UT, in the same format as Fig. 2. A dotted black rectangle shows the 5-min period used for the Walén analysis (16:36:03–16:41:03 UT, See Fig. 7), and the two grey-hatched periods correspond to the lobe/mantle ions (16:36:03–16:36:15 UT) and the faster magnetosheath-like ions (16:37:51–16:38:15 UT) whose phase space densities are presented in Fig. 6

identified by visual inspection. All cases took place in the southern hemisphere, as characterised by the negative values of the B_X component in the lobe/mantle region (Fig. 4). We found that $(V - V_{HT})$ and V_A are negatively correlated in all cases. The Walén slope is between -0.4 and -0.6 in 14 of the 17 cases, around -0.3 in 2 cases and ~ -0.8 in 1. This result shows that most encounters with faster anti-sunward flows can be attributed to crossings of open magnetopause boundaries where magnetosheath ions enter through open field lines generated by magnetic reconnection at the dayside magnetopause.

Global MHD simulation

We performed a global magnetohydrodynamic (MHD) simulation using the SWMF/BATS-R-US code with the Rice Convection Model (Tóth et al. 2005, 2012) to estimate the entire shape of the magnetosphere during this event (Figs. 8, 9 and 10). The GSM coordinate system is used for the simulation study. The OMNI solar wind data including the longitudinal and latitudinal flow components were used as upstream parameters for the simulation, while B_X was fixed to 3.708 nT which is the average value between 14:30 and 14:40 UT. The density contour and the bulk flow velocity vectors in the XY plane at 14:30 UT (Fig. 8a) show that the magnetotail is entirely shifted toward dawn in the simulation. The V_Y contour in the XY plane with flow lines (Fig. 8b) displays that the solar wind plasma flow is deflected toward dusk at the bow shock in front of the magnetosphere, which is consistent with our previous study (Nishino et al. 2008). The width of the magnetosheath on the duskside is larger than that on the dawnside, which is also consistent with this previous study.

Figure 9 shows the absolute value of the current density in the (a) XY and (b) XZ planes. The regions with higher current density are distributed near the bow shock, the magnetopause, and inside the magnetosphere. The location of the magnetopause in the XY plane based on a higher current density is consistent with the steep plasma density gradient between the magnetosheath and the magnetosphere. The magnetic tension of the draped field lines around the magnetosphere might pull the magnetotail toward dawn, resulting in the expansion of the magnetosphere observed on the dawnside. The current density in the XZ plane enhances near the dayside magnetopause, where the Cluster spacecraft was located. In the next section we will show data from the Cluster spacecraft which was located near the southern cusp.

Figure 10 displays (a) the plasma density and (b) the current density in the $X = -3.46 R_E$ plane, on which Geotail was located at 14:30 UT. In the simulation, the dawnward expansion of the magnetosphere is more significant in the southern hemisphere, which is caused by

an inclination of the magnetotail due to the negative IMF B_Y . The simulated magnetic field line at Geotail is connected to the southern polar cap on one side and the IMF on the other side. The open field line may be generated by magnetic reconnection at the dayside magnetopause.

These simulation results mean that the dawnward shift of the magnetotail is partly caused by the dusk-to-dawn component of the solar wind flow, but the V_Y component alone cannot explain all the deformation of the magnetotail. As presented by our previous study (Nishino et al. 2008), the low- M_A solar wind and Parker spiral IMF conditions are also essential factors that make the magnetotail skewed toward dawn. A north-south asymmetry of the magnetosheath width (Fig. 9b) may derive from a southward shift of the magnetotail that can be caused by a positive (sunward) IMF B_X (Cowley 1981) and a negative (southward) solar wind V_Z . The southward shift of the magnetotail might have affected magnetopause encounters by the Geotail spacecraft, since the widest region of the magnetotail in the dawn-dusk direction may also move toward south.

Cluster observations near southern cusp

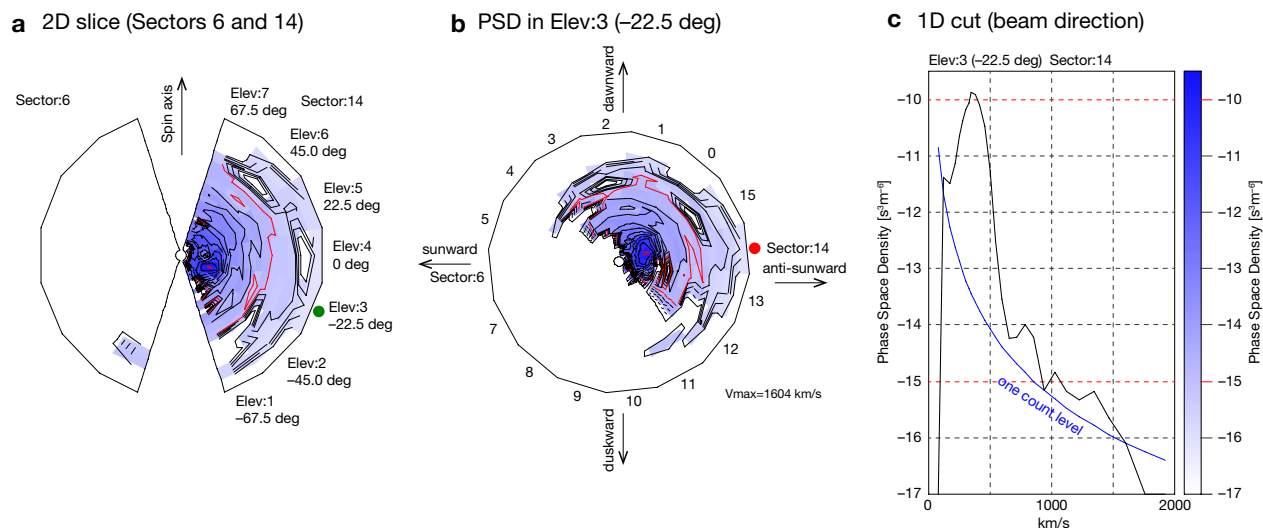
When Geotail observed the long-lasting boundary crossings at the flank on the dawnside, the Cluster spacecraft passed near the southern cusp region from the magnetosheath to the magnetosphere and encountered high-energy ion jets around the magnetopause. Figure 11 shows the plasma and magnetic field data from Cluster 1 (C1) and Cluster 3 (C3) from 13:30 to 17:00 UT for the same period as Fig. 4. The two spacecraft were separated by about $0.7 R_E$ in the Z direction, with C1 being closer to the Earth and C3 to the magnetosheath. The locations of C1 and C3 at 15:00 UT projected onto the GSM- XY plane are shown in Fig. 12.

Until 14:17 UT, C1 stayed in the magnetosheath, where B_Y was dominant, the plasma density was roughly $2\text{--}3 \text{ cm}^{-3}$, and the bulk ion flow was directed anti-sunward and southward. From 14:17 UT when C1 was located at $(10.9, 1.7, -11.0) R_E$, it detected anti-sunward and dawnward ion jets of $V_{jet} = (-330, -234, -151) \text{ km/s}$ with a speed of $\sim 430 \text{ km/s}$ accompanied by a stable sunward magnetic field of $(11, 0.7, 3.5) \text{ nT}$. The stable sunward magnetic field and the ion jets suggest that C1 came into the magnetopause boundary layer or the dayside magnetosphere. The ion jets in the magnetopause boundary layer had a density as low as 1.4 cm^{-3} , and they were possibly exhausts from dayside magnetic reconnection.

At almost the same time as C1 experienced the magnetopause crossing, C3 still stayed in the magnetosheath. The observed values in the magnetosheath by C3 at 14:15 UT were as follows: The plasma flow was

Geotail LEP/EAi (3D) Ion phase space density

2007-02-11 16:37:51–16:38:15 UT (Magnetosheath, 2 data sets accumulated)



2007-02-11 16:36:03–16:36:15 UT (Lobe/mantle)

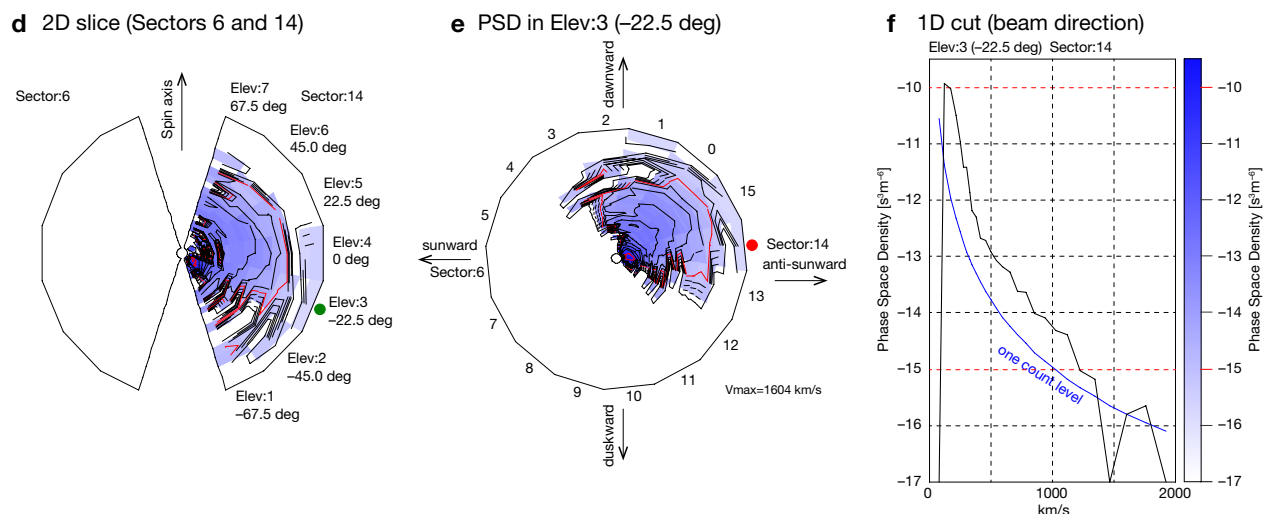
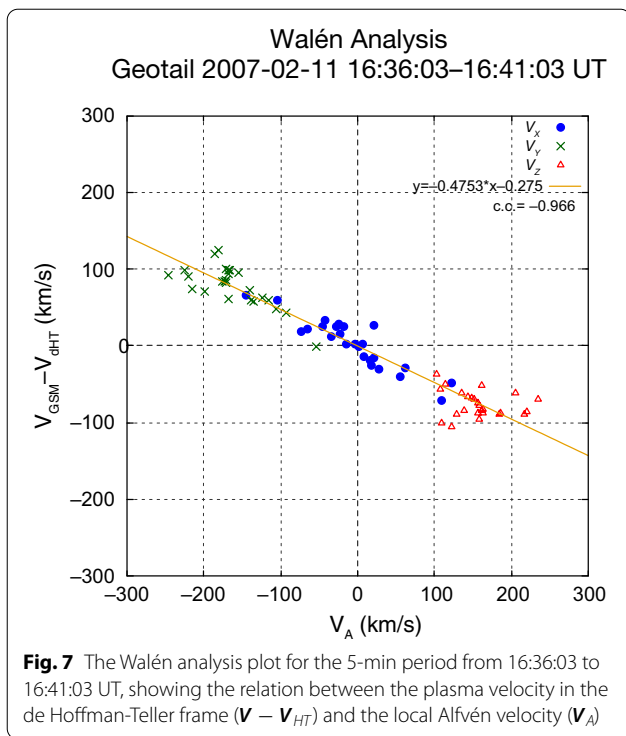


Fig. 6 Ion phase space density for the 24-s period from 16:37:51 to 16:38:15 UT in the unit of $s^3 m^{-6}$. **a** The two-dimensional slice of the ion phase space density, showing the anti-sunward beam component. The plane includes the spin axis (close to the GSE Z direction), Sector 14 (close to the anti-sunward direction) with the peak of the phase space density and Sector 6 (opposite to Sector 14; close to the sunward direction). **b** The ion phase space density at Elevation 3 which is directed 22.5° southward of the GSE XY plane and includes the peak of the anti-sunward beam component. **c** The one-dimensional cut of the ion phase space density in the direction of the anti-sunward beam component (Sector 14 and Elevation 3). (See Mukai et al. (1994) for the details of the LEP-EAi instrument.) Ion phase space density taken in the lobe/mantle region from 16:36:03 to 16:36:15 UT is shown in Panels **d–f** in the same format as above. The colour scales for the phase space density in 6 panels are identical. Logarithmic is presented on the right side

$V_{SH} \sim (-150, 15, -66)$ km/s with a speed of ~ 160 km/s. The magnetic field was (3.6, -14, 0.4) nT with a strength of 15 nT; the dominating dusk-to-dawn component may result from a draping of the IMF around the magnetosphere. The ion density was $\sim 2.4 \text{ cm}^{-3}$ and the parallel

and perpendicular ion temperatures were 11 eV and 38 eV, respectively. The corresponding ion beta values were 0.05 in the parallel direction and 0.17 in the perpendicular direction, which means that the plasma on the magnetosheath side had a very low beta ($\beta \ll 1$).

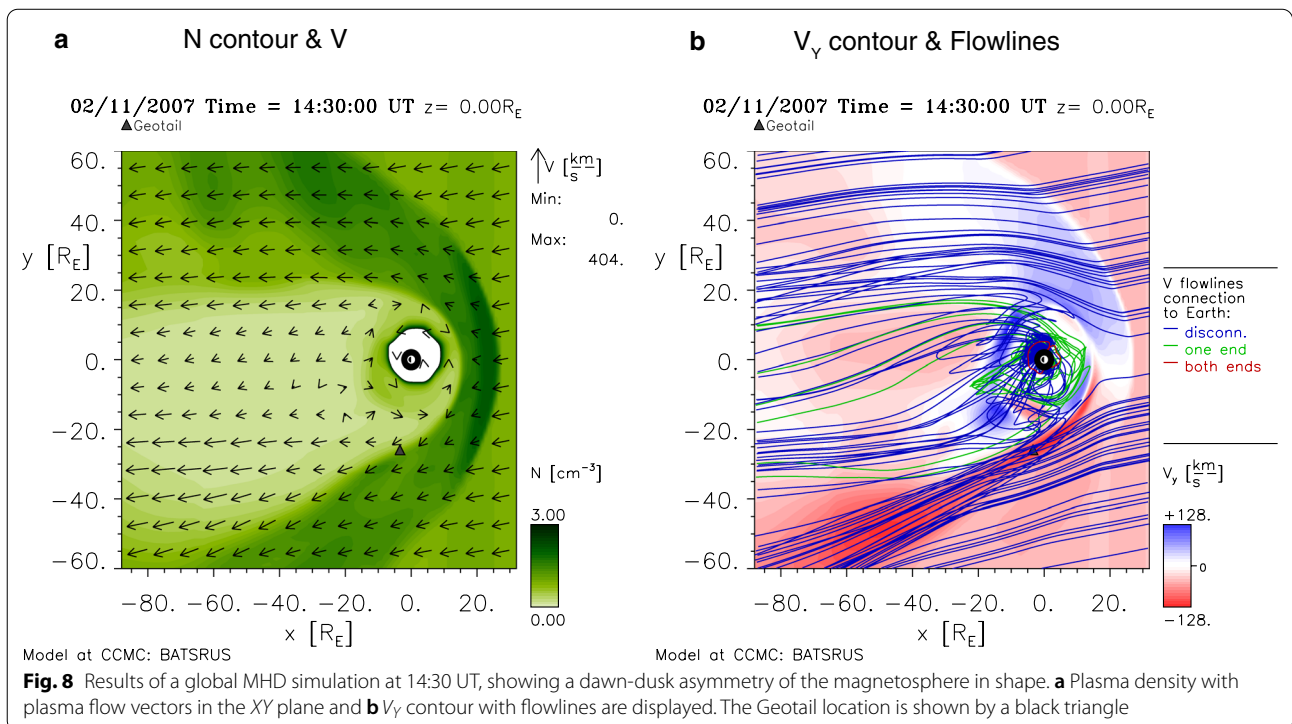


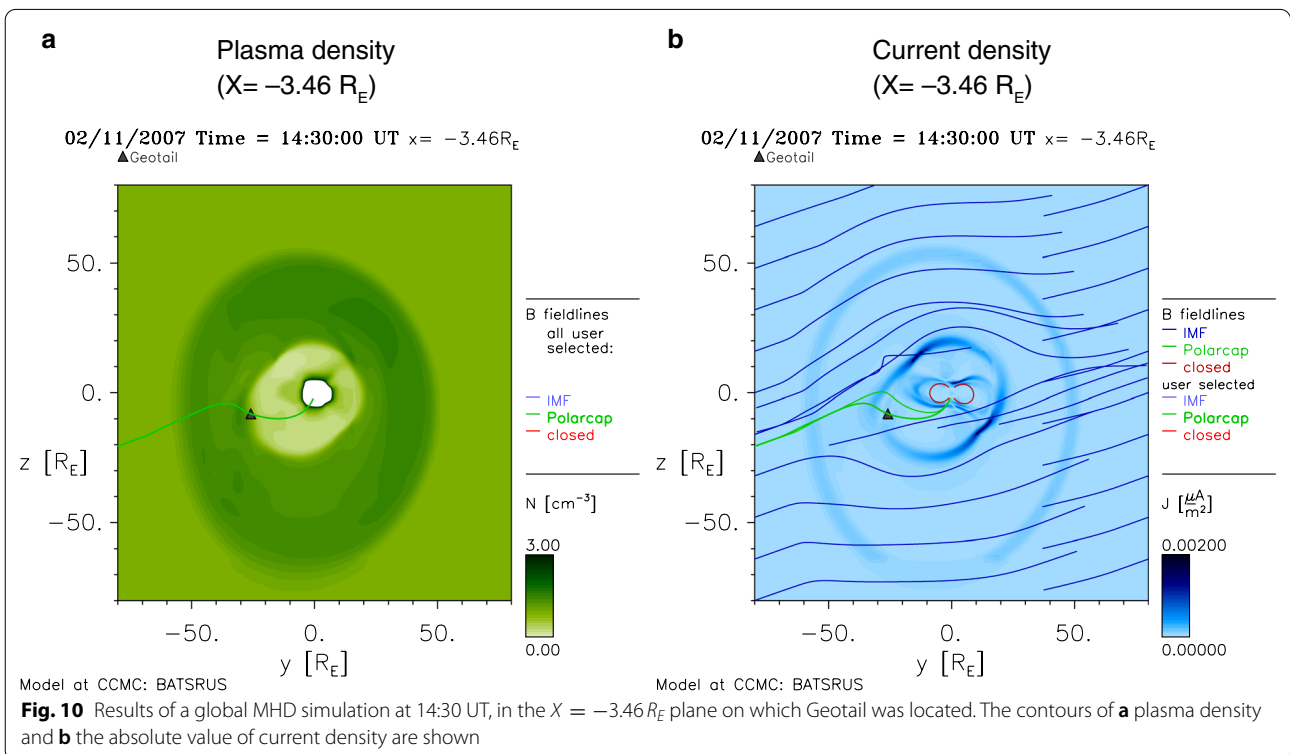
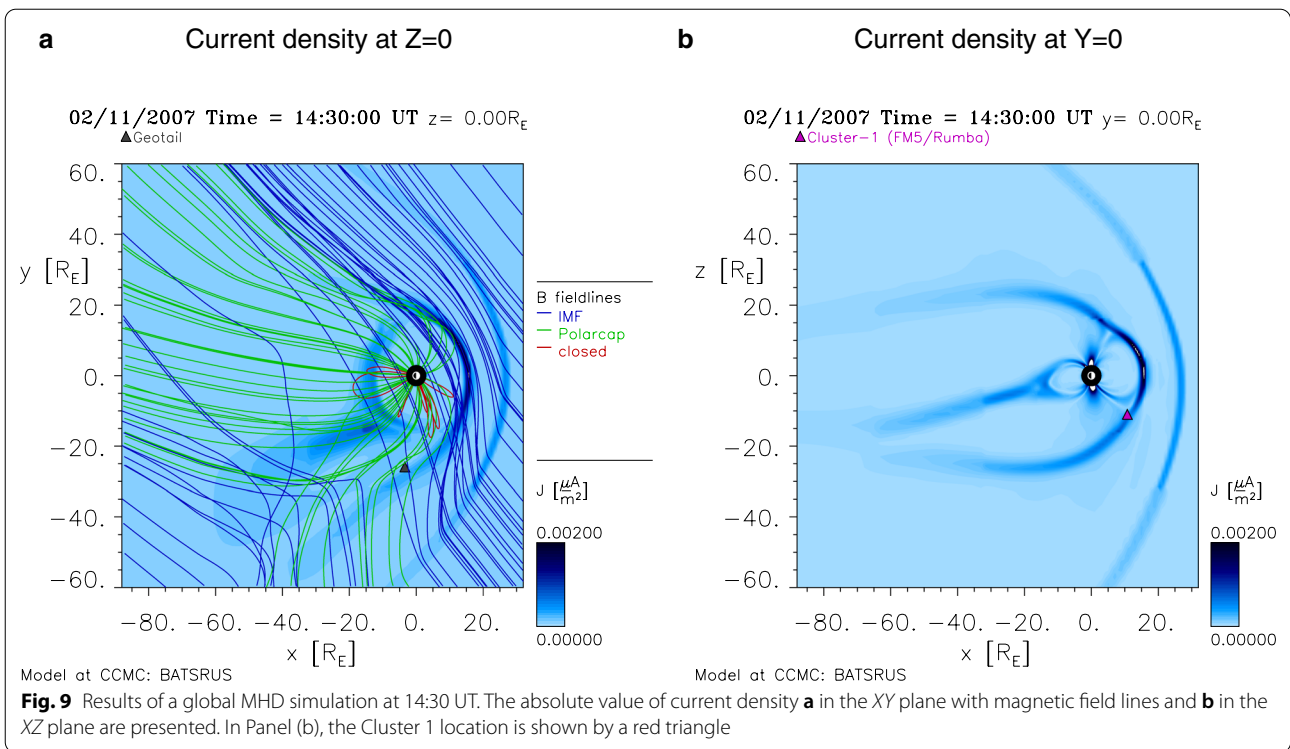
The difference between the reconnection jet at C1 (\mathbf{V}_{jet}) and the magnetosheath flow at C3 (\mathbf{V}_{SH}) (i.e. $\mathbf{V}_{jet} - \mathbf{V}_{SH}$) was $(-180, -249, -85)$ km/s and its absolute value

was 320 km/s. The combination of the magnetic field strength of 15 nT and the plasma density of 1.4 cm^{-3} yields a reconnection Alfvén speed of ~ 250 km/s, which is roughly in the same order as the ion jet speed. C3 also began to detect anti-sunward ion jets at 14:28 UT, when it was located at $(10.4, 1.3, -11.8) R_E$. After detecting a sunward and northward ion jet at 14:50 UT, C3 continuously detected anti-sunward ion jets from 14:59 to 15:51 UT.

The magnetic field in the boundary layer observed by Cluster were highly fluctuating, and in particular its strength decreased significantly. The decreases in the magnetic field strength (e.g. at 14:50 UT) were accompanied by ion flow reversals, which suggests that the spacecraft was located near a reconnection X-line. These features contrast with Geotail observations of stable magnetic field intensity and only anti-sunward (tailward) ion jets.

Analysis of magnetic reconnection itself is beyond the scope of this paper, but here we suggest that magnetic reconnection occurred continuously at the dayside magnetopause, based on the Cluster observations. The frequent occurrence of magnetic reconnection at the magnetopause under such low beta conditions in the magnetosheath is consistent with a previous statistical study (Phan et al. 2013).





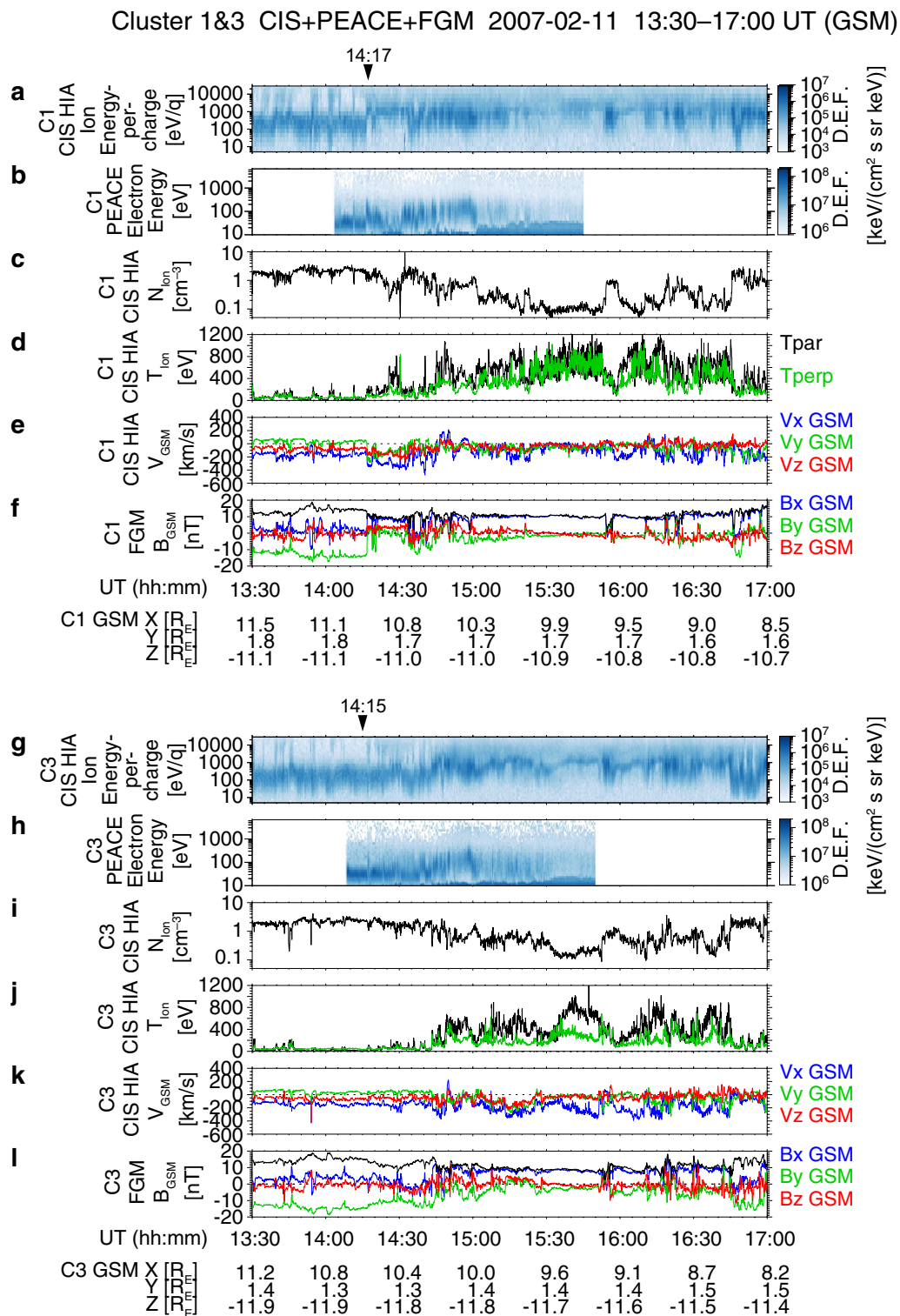
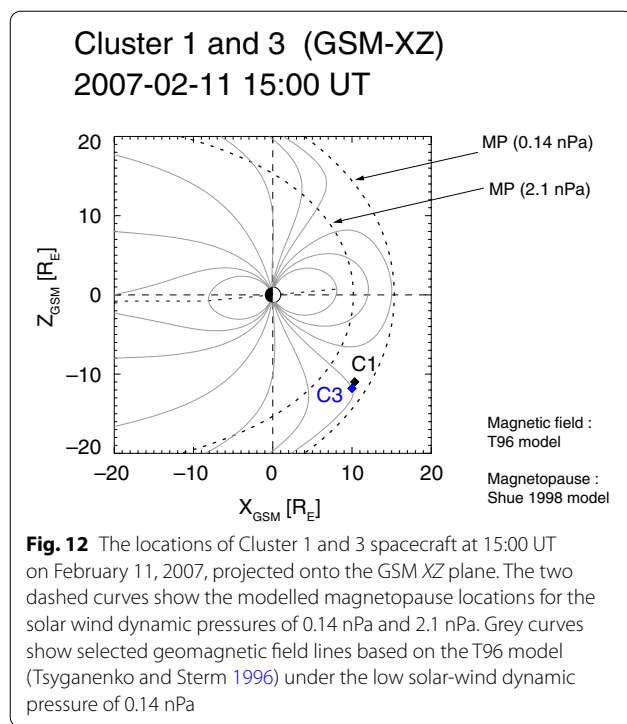


Fig. 11 Cluster 1 and 3 observations from 13:30 to 17:00 UT on February 11, 2007, including southern high-latitude magnetopause encounters. From the top, **a** omni-directional ion energy-time spectrogram, **b** omni-directional electron energy-time spectrogram, **c** ion density, **d** ion temperature, **e** ion velocity, **f** magnetic field from Cluster 1. **g-l** Data from Cluster 3 are plotted in the same format



Discussion and conclusions

This paper shows that a dawn-dusk asymmetric deformation of the magnetosphere expanding toward dawn occurs under the very low- M_A solar wind and Parker spiral IMF conditions. Although the dawnward expansion of the magnetosphere was predicted in the global simulation of our previous study, this study provides the first in situ observations consistent with the dawn-dusk magnetospheric deformation when the solar-wind M_A was as low as ~ 2 . We confirmed that the entire dawnward shift of the magnetotail was partly due to the dusk-to-dawn component of the solar wind flow and partly due to the ‘magnetic effect’ that typically occurs under low- M_A conditions (Nishino et al. 2008; Lavraud et al. 2013). On the other hand, the width of the magnetosheath on the dawnside becomes narrower than that on the duskside. The slight north-south asymmetry of the magnetosheath width (Fig. 6b) may result from the positive (sunward) IMF B_X and the negative (southward) solar wind V_Z .

The frequent jumps at the magnetopause of the ion velocity between the magnetosheath high-speed values and lobe/mantle lower-speed values, observed by Geotail, are consistent with magnetosheath plasma entry through open field lines generated by magnetic reconnection at the dayside magnetopause, as supported by the results of the Walén analysis. The generation mechanism of the magnetosheath flow much faster than the upstream solar wind is unsolved in this study. It has

been shown that the magnetic pressure gradient and tension forces by the draped IMF around the magnetosphere under the low- M_A solar wind can accelerate the magnetosheath plasma (Lavraud et al. 2007; Lavraud and Borovsky 2008). However, under the Parker-spiral IMF configuration with a small B_Z component, the plasma acceleration by this effect is expected to occur in the high-latitude region rather than at the flanks. Some local acceleration due to complicated magnetic field structures in the magnetosheath might take place, which is beyond the scope of this study.

When the anti-sunward ion flows were detected by Geotail, high-energy electrons were not detected there. One possibility for the lack of high-energy electrons is that electrons accelerated by magnetic reconnection may have a much faster speed than protons, and thus high-energy electrons go away promptly along the magnetic field lines and cannot be detected by Geotail located far from the X-line. This scenario is analogous to the lack of energetic magnetospheric electrons in the deep plasma sheet where low-energy ions from magnetosheath and high-energy magnetospheric ions coexist as a result of plasma mixing (Phan et al. 2000).

The repetitive encounters of the denser magnetosheath-like regions in the boundary layer might be caused by surface waves generated by interactions between the magnetosheath flow and the magnetopause or by turbulent flows downstream of the quasi-parallel bow shock on the dawnside under Parker-spiral IMF orientation. Another possibility for the repetitive encounters with magnetosheath-like flows is ion acceleration by magnetic reconnection associated with Kelvin–Helmholtz (KH) vortices at the magnetopause. However, the magnetic field for the period of multiple boundary crossings did not show significant variations in strength, which is not consistent with previous observations of fluctuating magnetic field strength in the KH vortices (Hasegawa et al. 2006). The very low beta environment of the magnetosheath may prevent the KH instability from developing into the non-linear stage (Miura 1984; Kavosi and Raeder 2015).

Our observations of the magnetospheric deformation and plasma acceleration under low- M_A solar wind and obliquely directed magnetic field conditions may be applicable to other solar system objects, exoplanets (Lugaz et al. 2016) and the interstellar medium (Miniati et al. 1999). Significant deformation of the planetary and exoplanetary magnetospheres may affect interactions between the low- M_A solar/stellar wind and the magnetospheres. In particular, the present results encourage studying the environment around the planet Mercury, where low- M_A solar wind is expected (Slavin and Holzer 1981; Sun et al. 2022). The BepiColombo spacecraft arriving at

Mercury in late 2025 (Benkhoff et al. 2021) can provide valuable information on the asymmetric deformations of the small magnetosphere under the lower M_A , which may help us understand exoplanetary magnetospheric environments as well.

Abbreviations

M_A : Alfvén Mach number; GSE: Geocentric solar ecliptic; GSM: Geocentric solar magnetospheric; IMF: Interplanetary magnetic field; KH: Kelvin–Helmholtz; MHD: Magnetohydrodynamics.

Acknowledgements

The authors are grateful to all members of the Geotail project. The authors thank the principal investigators of the Wind spacecraft for providing solar wind data through CDAWeb at NASA, and thank the principal investigators of the Cluster spacecraft for providing plasma and magnetic field data through the Cluster Science Archive website of European Space Agency (ESA). The authors gratefully acknowledge the development team of the Space Physics Environment Data Analysis System (SPEDAS) software (Angelopoulos et al. 2019). The work of M. N. Nishino was supported by JSPS KAKENHI grant no. 19K03947. The work of Y. Miyashita was supported by Korea Astronomy and Space Science Institute under the R & D program (2022-1-850-09) supervised by the Ministry of Science and ICT. M. Nowada has been supported by a grant of the National Natural Science Foundation of China (grant no. NSFC 42074194). Work at LAB was performed with support from CNRS, CNES, and Univ. Bordeaux. Three anonymous reviewers are highly acknowledged for their constructive comments and suggestions on improving the study, particularly the data analysis of fast ion flows around the dawnside magnetopause.

Author contributions

MNN designed this study and wrote the manuscript. HH significantly contributed to the interpretation of the data analysis results. YS provided original data and widely contributed to the work. YM provided graphical procedures. SK provided computational programs for data analysis. All authors attended the scientific discussion. All authors read and approved the final manuscript.

Funding

This work was supported by JSPS KAKENHI Grant Number 19K03947, Korea Astronomy and Space Science Institute under the R & D program (2022-1-850-09) supervised by the Ministry of Science and ICT, and a grant of the National Natural Science Foundation of China (NSFC 42074194).

Availability of data and materials

Geotail data are available from the DARTS website (<https://darts.isas.jaxa.jp/stp/geotail/data.html>). Solar wind data from the Wind spacecraft are provided by CDAWeb of NASA (<https://cdaweb.gsfc.nasa.gov/>). The global MHD simulation of the magnetosphere was carried out using the Space Weather Modeling Framework (SWMF) and the Block Adaptive Tree Solar wind Roe-type Upwind Scheme (BATS-R-US) tools developed at the University of Michigan's Center for Space Environment Modeling (CSEM). The modelling tools used in this publication are available online through the University of Michigan to download and are available at the Community Coordinated Modeling Center (CCMC) at NASA Goddard Space Flight Center. All simulation data presented in this study have been provided by the CCMC through their public Runs on Request system and are available at https://ccmc.gsfc.nasa.gov/results/viewrun.php?domain=GM&runnumber=Masaki_Nishino_082019_1.

Declarations

Ethics approval and consent to participate

Not applicable.

Consent for publication

Not applicable.

Competing interests

The authors declare that they have no competing interests.

Author details

¹Department of Earth and Planetary Science, Graduate School of Science, University of Tokyo, 7-3-1 Hongo, Bunkyo-ku, Tokyo 113-0033, Japan. ²Institute of Space and Astronautical Science, Japan Aerospace Exploration Agency, 3-1-1 Yoshinodai, Chuo-ku, Sagami-hara 252-5210, Japan. ³Faculty of Science, Gakushuin University, 1-5-1 Mejiro, Toshima-ku, Tokyo 171-8588, Japan. ⁴Laboratoire d'astrophysique de Bordeaux, Université de Bordeaux, CNRS, B18N, allée Geoffroy Saint-Hilaire, 33615 Pessac, France. ⁵Korea Astronomy and Space Science Institute, 776 Daedeok-daero, Yuseong-gu, Daejeon 34055, South Korea. ⁶Department of Astronomy and Space Science, Korea University of Science and Technology, Daejeon, South Korea. ⁷Shandong Key Laboratory of Optical Astronomy and Solar-Terrestrial Environment, School of Space Science and Physics Institute of Space Sciences, Shandong University, 180 Wen-Hua West Road, Weihai 264209, Shandong, People's Republic of China. ⁸Tokyo, Japan.

Received: 10 June 2022 Accepted: 28 November 2022

Published online: 09 December 2022

References

- Acuña MH, Ogilvie KW, Baker DN, Curtis SA, Fairfield DH, Mish WH (1995) The Global Geospace Science Program and its investigations. *Space Sci Rev* 71:5–21. <https://doi.org/10.1007/BF00751323>
- Angelopoulos V, Cruce P, Drozdov A et al (2019) The Space Physics Environment Data Analysis System (SPEDAS). *Space Sci Rev* 215:9. <https://doi.org/10.1007/s11214-018-0576-4>
- Balogh A, Dunlop MW, Cowley SWH, Southwood DJ, Thomlinson JG, Glassmeier KH, Musmann G, Lühr H, Buchert S, Acuña MH, Fairfield DH, Slavin JA, Riedler W, Schwingenschuh H, Kivelson MG (1997) The Cluster magnetic field investigation. *Space Sci Rev* 79:65–91. <https://doi.org/10.1023/A:1004970907748>
- Benkhoff J, Murakami G, Baumjohann W, Besse S, Bunce E, Casale M, Cremese G, Glassmeier K-H, Hayakawa H, Heyner D, Hiesinger H, Huovelin J, Hussmann H, Iafolla V, Iess L, Kasaba Y, Kobayashi M, Milillo A, Mitrofanov IG, Montagnon E, Novara M, Orsini S, Quemerais E, Reininghaus U, Saito Y, Santoli F, Stramaccioni D, Sutherland O, Thomas N, Yoshikawa I, Zender J (2021) BepiColombo—Mission overview and science goals. *Space Sci Rev* 217:90. <https://doi.org/10.1007/s11214-021-00861-4>
- Chané E, Saur J, Neubauer FM, Raeder J, Poedts S (2012) Observational evidence of Alfvén wings at the Earth. *J Geophys Res* 117:A09217. <https://doi.org/10.1029/2012JA017628>
- Chapman JF, Cairns IH, Lyon JG, Boshuizen CR (2004) MHD simulations of Earth's bow shock: interplanetary magnetic field orientation effects on shape and position. *J Geophys Res* 109:A04215. <https://doi.org/10.1029/2003JA010235>
- Cowley SWH (1981) Asymmetry effects associated with the x-component of the IMF in a magnetically open magnetosphere. *Planet Space Sci* 29:809–818. [https://doi.org/10.1016/0032-0633\(81\)90071-4](https://doi.org/10.1016/0032-0633(81)90071-4)
- Dandouras I, Barthe A, Penou E, Brunato S, Réme H, Kistler LM, Bavassano-Cattaneo MB, Blagau A (2010) Cluster Ion Spectrometry (CIS) data in the Cluster Active Archive (CAA). In: Laakso H, Taylor M, Escoubet C (eds) The Cluster Active Archive. Astrophysics and space science proceedings (chap. 3). Springer, Dordrecht, pp 51–72. https://doi.org/10.1007/978-90-481-3499-1_3
- Fairfield DH, Cairns Iver H, Desch MD, Szabo A, Lazarus AJ, Aellig MR (2001) The location of low Mach number bow shocks at Earth. *J Geophys Res* 106:25361–25376. <https://doi.org/10.1029/2000JA000252>
- Fazakerley AN, Lahiff AD, Wilson RJ, Rozum I, Anekallu C, West M, Bacai H (2010) PEACE data in the Cluster Active Archive. In: Laakso H, Taylor M, Escoubet C (eds) The Cluster Active Archive. Astrophysics and space science proceedings. Springer, Dordrecht, pp 129–144. https://doi.org/10.1007/978-90-481-3499-1_8
- Hasegawa H, Maezawa K, Mukai T, Saito Y (2002) Plasma entry across the distant tail magnetopause, 1. Global properties and IMF dependence. *J Geophys Res* 107:1063. <https://doi.org/10.1029/2001JA900139>

- Hasegawa H, Maezawa K, Mukai T, Saito Y (2002) Plasma entry across the distant tail magnetopause, 2. Comparison between MHD theory and observation. *J Geophys Res* 107:1073. <https://doi.org/10.1029/2001JG100138>
- Hasegawa H, Fujimoto M, Takagi K, Saito Y, Mukai T, Réme H (2006) Single-spacecraft detection of rolled-up Kelvin–Helmholtz vortices at the flank magnetopause. *J Geophys Res* 111:A09203. <https://doi.org/10.1029/2006JA011728>
- Janardhan P, Fujiki K, Kojima M, Tokumaru M, Hakamata K (2005) Resolving the enigmatic solar wind disappearance event of 11 May 1999. *J Geophys Res* 110:A08181. <https://doi.org/10.1029/2004JA010535>
- Jia X, Kivelson MG (2021) The magnetosphere of Ganymede. In: Maggiolo R, Andre N, Hasegawa H, Welling DT, Zhang Y, Paxton LJ (eds) Magnetospheres in the Solar System. Space physics and aeronomy collection, vol 2. American Geophysical Union, pp 557–573. <https://doi.org/10.1002/9781119815624.ch35>
- Johnstone AD, Alsop C, Borge S, Carter PJ, Coates AJ, Coker AJ, Fazakerley AN, Grande M, Gowen RA, Gurgiolo C, Hancock BK, Narheim B, Preece A, Sheather PH, Winningham JD, Woodliffe RD (1997) PEACE: a plasma electron and current experiment. *Space Sci Rev* 79:351–398. <https://doi.org/10.1023/A:1004938001388>
- Kataoka R, Miyoshi Y (2008) Magnetosphere inflation during the recovery phase of geomagnetic storms as an excellent magnetic confinement of killer electrons. *Geophys Res Lett* 35:L06S09. <https://doi.org/10.1029/2007GL031842>
- Kavosi S, Raeder J (2015) Ubiquity of Kelvin–Helmholtz waves at Earth's magnetopause. *Nat Commun* 6:7019. <https://doi.org/10.1038/ncomms8019>
- Kokubun S, Yamamoto T, Acuña MH, Hayashi K, Shiokawa K, Kawano H (1994) The Geotail magnetic field experiment. *J Geomag Geoelectr* 46:7–21. <https://doi.org/10.5636/jgg.46.7>
- Lavraud B, Borovsky JE, Ridley AJ, Pogue EW, Thomsen MF, Réme H, Fazakerley AN, Lucek EA (2007) Strong bulk plasma acceleration in Earth's magnetosheath: a magnetic slingshot effect? *Geophys Res Lett* 34:L14102. <https://doi.org/10.1029/2007GL030024>
- Lavraud B, Borovsky JE (2008) Altered solar wind-magnetosphere interaction at low Mach numbers: Coronal mass ejections. *J Geophys Res* 113:A00808. <https://doi.org/10.1029/2008JA013192>
- Lavraud B, Larroque E, Budnik E, Génot V, Borovsky JE, Dunlop MW, Fougère C, Hasegawa H, Jacquy C, Nykyri K, Ruffenach A, Taylor MGGT, Dandouras I, Réme H (2013) Asymmetry of magnetosheath flows and magnetopause shape during low Alfvén Mach number solar wind. *J Geophys Res* 118:1089–1100. <https://doi.org/10.1002/jgra.50145>
- Le G, Russell CT, Petrinec SM (2000) The magnetosphere on May 11, 1999, the day the solar wind almost disappeared: I. Current systems. *Geophys Res Lett* 27:1827–1830. <https://doi.org/10.1029/1999GL010774>
- Lepping RP, Acuña MH, Burlaga LF et al (1995) The WIND magnetic field investigation. *Space Sci Rev* 71:207–229. <https://doi.org/10.1007/BF00751330>
- Lin RP, Anderson KA, Ashford S, Carlson C, Curtis D, Ergun R et al (1995) A three-dimensional plasma and energetic particle investigation for the wind spacecraft. *Space Sci Rev* 71:125–153. <https://doi.org/10.1007/BF00751328>
- Lugaz N, Farrugia C, Huang CL, Winslow RM, Spence HE, Schwadron NA (2000) Earth's magnetosphere and outer radiation belt under sub-Alfvénic solar wind. *Nat Commun* 7:13001. <https://doi.org/10.1038/ncomms13001>
- Miniati F, Jones TW, Ryu D (1999) On the exchange of kinetic and magnetic energy between clouds and the interstellar medium. *Astrophys J* 517:242. <https://doi.org/10.1086/307162>
- Miura A (1984) Anomalous transport by magnetohydrodynamic Kelvin–Helmholtz instabilities in the solar wind-magnetosphere interaction. *J Geophys Res* 89:801–818. <https://doi.org/10.1029/JA089iA02p00801>
- Mukai T, Machida S, Saito Y, Hirahara M, Terasawa T, Kaya N, Obara T, Ejiri M, Nishida A (1994) The Low Energy Particle (LEP) experiment onboard the Geotail satellite. *J Geomag Geoelectr* 46:669–692. <https://doi.org/10.5636/jgg.46.669>
- Nishino MN, Fujimoto M, Phan TD, Mukai T, Saito Y, Kuznetsova MM, Rastätter L (2008) Anomalous flow deflection at Earth's low-Alfvén-Mach-number bow shock. *Phys Rev Lett* 101:065003. <https://doi.org/10.1103/PhysRevLett.101.065003>
- Phan TD, Lin RP, Fuselier SA, Fujimoto M (2000) Wind observations of mixed magnetosheath-plasma sheet ions deep inside the magnetosphere. *J Geophys Res* 105:5497. <https://doi.org/10.1029/1999JA900455>
- Phan TD, Paschmann G, Gosling JT, Øieroset M, Fujimoto M, Drake JF, Angelopoulos V (2013) The dependence of magnetic reconnection on plasma β and magnetic shear: evidence from magnetopause observations. *Geophys Res Lett* 40:11–16. <https://doi.org/10.1029/2012GL054528>
- Rème H, Bosqued JM, Sauvaud JA, Cros A, Dandouras J, Aoustin C, Bouysou J, Camus Th, Cuvilo J, Martz C, Médale JL, Perrier H, Romefort D, Rouzaud J, D'Uston C, Möbius E, Crocker K, Granoff M, Kistler LM, Poptek M, Hovestadt D, Klecker B, Paschmann G, Scholer M, Carlson CW, Curtis DW, Lin RP, Mcfadden JP, Formisano V, Amata E, Bavassano-Cattaneo MB, Baldetti P, Belluci G, Bruno R, Chionchio G, Di Lellis A, Shelley EG, Ghielmetti AG, Lennartsson W, Korth A, Rosenbauer H, Lundin R, Olsen S, Parks GK, McCarthy M, Balsiger H (1997) The cluster ion spectrometry (CIS) experiment. *Space Sci Rev* 79:303–350. <https://doi.org/10.1023/A:1004929816409>
- Shue JH, Song P, Russell CT, Steinberg JT, Chao JK, Zastenker G, Vaisberg OL, Kokubun S, Singer HJ, Detman TR, Kawano H (1998) Magnetopause location under extreme solar wind conditions. *J Geophys Res* 103:17691–17700. <https://doi.org/10.1029/98JA01103>
- Slavin JA, Holzer RE (1981) Solar wind flow about the terrestrial planets 1. Modeling bow shock position and shape. *J Geophys Res* 86(A13):11401–11418. <https://doi.org/10.1029/JA086iA13p11401>
- Sonnerup BUÖ, Papamastorakis I, Paschmann G, Lühr H (1987) Magnetopause properties from AMPTE/IRM observations of the convection electric field: Method development. *J Geophys Res* 92:12137–12159. <https://doi.org/10.1029/JA092iA11p12137>
- Sun W, Dewey RM, Aizawa S, Huang J, Slavin JA, Fu S, Wei Y, Bowers CF (2022) Review of Mercury's dynamic magnetosphere: post-MESSENGER era and comparative magnetospheres. *Sci China Earth Sci* 65(1):25–74. <https://doi.org/10.1007/s11430-021-9828-0>
- Tóth G, Sokolov IV, Gombosi TI, Chesney DR, Clauer CR, De Zeeuw DL, Hansen KC, Kane KJ, Manchester WB, Oehmke RC, Powell KG, Ridley AJ, Roussev II, Stout QF, Volberg O, Wolf RA, Sazykin S, Chan A, Yu B, Kóta J (2005) Space weather modeling framework: a new tool for the space science community. *J Geophys Res* 110:A12226. <https://doi.org/10.1029/2005JA011126>
- Tóth G, van der Holst B, Sokolov IV, De Zeeuw DL, Gombosi TI, Fang F, Manchester WB, Meng X, Najib D, Powell KG, Stout QF, Glocer A, Ma Y-J, Opher M (2012) Adaptive numerical algorithms in space weather modeling. *J Comput Phys* 231:870–903. <https://doi.org/10.1016/j.jcp.2011.02.006>
- Tsyganenko NA, Stern DP (1996) Modeling the global magnetic field of the large-scale Birkeland current systems. *J Geophys Res* 101:27187–27198. <https://doi.org/10.1029/96ja02735>
- Watarai S, Watanabe T, Marubashi K (2001) Statistical analysis of long-duration low-density solar wind events. *Ann Geophys* 19:17–23. <https://doi.org/10.5194/angeo-19-17-2001>

Publisher's Note

Springer Nature remains neutral with regard to jurisdictional claims in published maps and institutional affiliations.

Submit your manuscript to a SpringerOpen® journal and benefit from:

- Convenient online submission
- Rigorous peer review
- Open access: articles freely available online
- High visibility within the field
- Retaining the copyright to your article

Submit your next manuscript at ► [springeropen.com](https://www.springeropen.com)